



HAL
open science

Why is NanoSIMS elemental imaging of arsenic in seaweed (*Laminaria digitata*) important for understanding of arsenic biochemistry in addition to speciation information?

E. Ender, M. Subirana, A. Raab, E. Krupp, Dirk Schaumlöffel, J. Feldmann

► To cite this version:

E. Ender, M. Subirana, A. Raab, E. Krupp, Dirk Schaumlöffel, et al.. Why is NanoSIMS elemental imaging of arsenic in seaweed (*Laminaria digitata*) important for understanding of arsenic biochemistry in addition to speciation information?. *Journal of Analytical Atomic Spectrometry*, 2019, 34, pp.2295 - 2302. 10.1039/C9JA00187E . hal-02320513

HAL Id: hal-02320513

<https://univ-pau.hal.science/hal-02320513>

Submitted on 9 Dec 2020

HAL is a multi-disciplinary open access archive for the deposit and dissemination of scientific research documents, whether they are published or not. The documents may come from teaching and research institutions in France or abroad, or from public or private research centers.

L'archive ouverte pluridisciplinaire **HAL**, est destinée au dépôt et à la diffusion de documents scientifiques de niveau recherche, publiés ou non, émanant des établissements d'enseignement et de recherche français ou étrangers, des laboratoires publics ou privés.

JAAS

Journal of Analytical Atomic Spectrometry

Accepted Manuscript

This article can be cited before page numbers have been issued, to do this please use: E. Ender, M. A. Subirana, A. Raab, E. Krupp, D. Schaumlöffel and J. Feldmann, *J. Anal. At. Spectrom.*, 2019, DOI: 10.1039/C9JA00187E.



This is an Accepted Manuscript, which has been through the Royal Society of Chemistry peer review process and has been accepted for publication.

Accepted Manuscripts are published online shortly after acceptance, before technical editing, formatting and proof reading. Using this free service, authors can make their results available to the community, in citable form, before we publish the edited article. We will replace this Accepted Manuscript with the edited and formatted Advance Article as soon as it is available.

You can find more information about Accepted Manuscripts in the [Information for Authors](#).

Please note that technical editing may introduce minor changes to the text and/or graphics, which may alter content. The journal's standard [Terms & Conditions](#) and the [Ethical guidelines](#) still apply. In no event shall the Royal Society of Chemistry be held responsible for any errors or omissions in this Accepted Manuscript or any consequences arising from the use of any information it contains.

Why is NanoSIMS elemental imaging of arsenic in seaweed (*Laminaria digitata*) important for understanding of arsenic biochemistry in addition of speciation information?

E. Ender¹, M.A.Subirana², A. Raab¹, E.M. Krupp¹, D. Schaumlöffel², J. Feldmann¹

¹TESLA, School of Natural and Computing Sciences, University of Aberdeen, Aberdeen AB24 3UE, Scotland, UK

²CNRS / Université de Pau et des Pays de l'Adour / E2S UPPA, Institut des Sciences Analytiques et de Physico-Chimie pour l'Environnement et les Matériaux, UMR 5254, 64000 Pau, France

Abstract

Brown seaweed such as *Laminaria digitata* is known to accumulate arsenic to more than 100 mg/kg. How the algae can tolerate such high level of arsenic has traditionally been studied by arsenic speciation analysis using HPLC-ICPMS, but the knowledge of its molecular forms has not yet given any answers. Here we demonstrate for the first time that the combination of speciation analysis with high resolution imaging by NanoSIMS and TEM identifies not only the molecular structures of arsenic but also the location of arsenic in cells and cell substructures in a brown seaweed species.

The majority of 117 mg/kg arsenic in *L. digitata* fronds was in the form of inorganic arsenic (53%) and arsenosugars (32%) and only 1.5% of total arsenic as arsenolipids (mainly as AsHC and AsPL). The lateral resolution of 300 nm and the concentration of arsenic was high enough for the localization of arsenic in the cells of the seaweed using NanoSIMS. The majority of arsenic was found in the cell walls and cell membrane, while the inside of the cell was almost arsenic free, which is not expected if the majority of arsenic species are hydrophilic. The NanoSIMS images questions the integrity of the arsenic species during extraction for the speciation analysis and that inorganic arsenic is unlikely to occur freely in the seaweed. Whether inorganic arsenic and the arsenosugars are bound directly to the polymeric carbohydrates alginates or fucoidans in the seaweed is unclear and needs further investigations.

34 Introduction

View Article Online
DOI: 10.1039/C9JA00187E

35
36 The use of analytical atomic spectrometry and in particular ICPMS has been instrumental to
37 identify the molecular forms of arsenic in biological samples over nearly three decades. The
38 complex arsenic biochemistry of more than 100 naturally occurring organoarsenicals in
39 addition to arsenite and arsenate made it necessary to use various HPLC methods coupled to
40 ICPMS and ESI-MS detection in off-line or on-line mode to identify the full spectrum of
41 arsenic species in biological samples even without standards.ⁱ However, neither the
42 biosynthetic pathways nor the classification whether these metabolic transformations are
43 detoxification pathways for inorganic arsenic or the formation of beneficial arsenic
44 containing biomolecules have been elucidated; although credible suggestions have recently
45 been made about the arsenosugars.ⁱⁱ What is missing is the localisation of the arsenic inside
46 the cells in order to answer the above mentioned questions about the biochemistry of arsenic.

47
48 It is well known that seaweeds bioaccumulate large concentrations of arsenic from seawater
49 with bioconcentration factor between 1,000 and 100,000.ⁱⁱⁱ Seaweeds and in particular brown
50 macroalgae can reach concentrations up to 200 mg As/kg.^{iv} Most of the arsenic in seaweeds
51 is present as organoarsenicals in the form of arsenosugars (As-sugars), dimethylarsinic acid
52 (DMA) and also in the lipid soluble forms of arsenic containing hydrocarbons (AsHC), fatty
53 acids (AsFA) and phospholipids (AsPL)^{v,vi}. Only *Hijiki* spp^{vii} and *Laminaria digitata*^{viii,ix}
54 seem to contain large amounts of inorganic arsenic.

55
56 Here we would like to illustrate the complementary information of using detailed arsenic
57 speciation analysis and mapping of arsenic at sub-cellular level using the brown seaweeds
58 *Laminaria digitata* as examples to gain more detailed insight into the bioaccumulative
59 behaviour of arsenic especially when the arsenic species are known. Special attention will be
60 given to the differences in the sample preparation procedures. While often the samples are
61 freeze-dried before speciation analysis by HPLC-ICPMS is performed in order to report on
62 concentration relative to dry mass, is it important to have fresh samples available for
63 transmission electron microscope (TEM) and nanoscale secondary ion mass spectrometry
64 (NanoSIMS) analysis which need to be prepared by cryofixation using high-pressure freezing
65 followed by cryo-substitution and resin embedding. This is necessary in order to conserve the
66 cellular ultrastructure and to fix the elements and not distribute them at a sub-cellular level.

67

68 Experimental Section

70 Chemicals and reagents

71 All chemicals and reagents were purchased from Sigma-Aldrich (Saint-Quentin Fallavier,
72 France) unless stated otherwise. All solutions, dilutions and preparations were made with water
73 (18.2 MΩ cm) obtained from a Milli-Q system (Millipore, Bedford, Ma, USA) unless stated
74 otherwise. A 10 μL drop of an arsenic ICP Standard, 1000 μg/mL (PlasmaCAL, Villebon-sur-
75 Yvette, France), was dried on a silica wafer and used as standard for mass calibration and mass
76 resolution tuning for As in NanoSIMS.

77 Chemicals used for extraction were of lab-grade quality (Fisher, UK). Chemicals used for total
78 As determination were of trace-element grade (VWR, UK). HPLC grade methanol (Rathburn,
79 UK), ammonium carbonate (Sigma, UK) and formic acid (mass-spec quality, Fluka, UK) were
80 used for the preparation of HPLC eluents. Nitric acid (70 % p.a. Fisher, UK) and hydrogen
81 peroxide (32 % Fisher, UK) were used for extraction and digestion. For quantification of As-
82 species sodium dimethylarsinic acid (DMA, Chemservice, USA) was dissolved in deionized
83 water and diluted as necessary. Identification of anionic As-species was aided by species
84 standards of DMA, MA (Chemservice, USA), arsenite and arsenate (BDH, UK). Seaweed
85 CRM (ERM-CD-200) a brown algae *Fucus vesiculosus* was purchased from JRC-Institute for
86 Reference Materials and Measurements (Geel, Belgium).

88 Samples

89 Sampling was conducted at a beach south of Aberdeen, on the east coast of Scotland
90 (57.139856 N, -2.051430 W) in November 2018. Freshly washed ashore whole thalli of
91 *Laminaria digitata* were harvested.

93 Sample preparation for NanoSIMS and TEM

94 Sample preparation was conducted at the Microscopy and Histology Core Facility at the
95 University of Aberdeen. Two replicates of *L. digitata* were prepared. Algae discs of 4 mm
96 diameter were prepared with a biopsy punch and transferred into gold-plated copper specimen
97 carriers filled with hexadecane. High Pressure Freezing was then carried out using a Leica EM
98 ICE (Leica Microsystems, Milton Keynes, UK). For freeze substitution samples were post-
99 fixed with 2% osmium tetroxide (OsO₄) in acetone and transferred into an automatic freeze
100 substitution system (AFS 2, Leica Mircosystems) following the programme outlined in
101 Supplementary material. This was followed by resin embedding (Spurr's resin, TAAB, UK)

1
2
3 102 through a stepwise infiltration of the samples with a graded resin and acetone series (10, 30, 40, 50, 70, and 90% resin in acetone). Finally, embedded in 100% resin the samples were
4 103 50, 70, and 90% resin in acetone). Finally, embedded in 100% resin the samples were
5 104 polymerized at 60 °C for at least 24 hours. For TEM analysis, 90 nm sections were cut from
6 105 the resin blocks using a diamond knife (Diatome Ltd, Switzerland) on an ultra-microtome
7 106 (Leica UC6, Leica Microsystems) and placed onto copper grids (TAAB, UK). For NanoSIMS
8 107 analysis, 300 nm sections were cut by the same method and placed on silicon wafers (Wafer
9 108 Solution, Le Bourget du lac, France).

109 110 Sample preparation for totals arsenic analysis and speciation analysis

111 *Laminaria digitata* fronds were cleaned by scraping and washing off epiphytes and sediment, freeze
112 dried and ground with mortar and pestle to a fine powder. Only the young fronts were analysed.

113 114 *Extraction of lipophilic arsenic*

115 Algae (1 g) were extracted with hexane (2 × 5 mL), followed by CH₂Cl₂/MeOH (2:1 v/v, 2 ×
116 5 mL), and both extracts were evaporated to dryness. For speciation analysis only the MeOH
117 soluble part of the CH₂Cl₂/MeOH extract was used.

118 119 *Extraction of hydrophilic arsenic*

120 The procedure of Petursdottir *et al.*^x was used for the extraction. In brief 0.1 g algae were mixed
121 with 10 mL of extraction solution (1 % (v/v) nitric acid and 2 % (v/v) hydrogen peroxide) and
122 heated in a microwave (Mars5, CEM, UK) to 95°C for 30 min. The solution was centrifuged
123 and the supernatant used for determination of inorganic arsenic.

124 125 *Digestion method to determine total arsenic*

126 Total As was determined after standard microwave digestion with HNO₃/H₂O₂ using a Mars5
127 system (CEM, UK) in solid *L. digitata*. An ICPMS/MS (Agilent 8800, UK) was used in mass
128 shift mode to determine As on m/z 91 as AsO⁺.

129 130 *Determination of hydrophilic and lipophilic arsenic species*

131 Hydrophilic arsenic species were determined by using anion exchange HPLC-ICPMS/MS. The
132 parameters are given in the supplementary material. The lipophilic arsenic speciation was
133 performed by coupling reverse-phase HPLC simultaneously to ICPMS/MS and ESI-qTOF-MS
134 as described previously^{xi}. The details are given in the supplementary material.

135

136 TEM analysis

137 Samples were viewed on the transmission electron microscopes JEM 1400 plus (JEOL, UK) at
138 an accelerating voltage of 100 kV using an AMT UltraVUE camera. The TEM instrument was
139 used to determine quality of sample preparation and for high resolution imaging of sub-cellular
140 structures. Copper grids have been used for sample sections.

141

142 NanoSIMS analysis

143 A NanoSIMS 50L (Cameca, Gennevilliers, France) was used for high resolution secondary ion
144 mass spectrometry analysis. A primary Cs⁺ ion source served for the mapping of
145 electronegative elements. Detectors were tuned for carbon (¹²C₂⁻), nitrogen (¹²C¹⁴N⁻),
146 phosphorus (³¹P⁻), sulphur (³²S⁻) and arsenic (⁷⁵As⁻). As the concentration of As in the sample
147 was relatively low, an As standard was used for mass calibration and mass resolution tuning
148 process. Cs⁺ ions were implanted onto the sample surface in order to increase sensitivity. It
149 should be noted that N cannot be directly measured using NanoSIMS, therefore carbon-
150 nitrogen (CN⁻) cluster ions are measured to detect N in the sample. Images were acquired with
151 a raster size ranging of 35 µm, divided into 512 x 512 pixels with a dwell time of 10 ms per
152 pixel. Individual sample sections were located using the NanoSIMS Charged Coupled Device
153 (CCD) camera. The field of view of the CCD camera is about 500 × 600 µm and the optical
154 resolution around 1 µm, which allows for an overview of the sample and a selection of regions
155 of interest for NanoSIMS analysis.

156

157 Results and discussion

158

159 The arsenic concentration in the freeze-dried *L. digitata* was 117 +/- 30 mg As/kg (Table 1),
160 which is in the normal range as reported previously.^{viii} The accuracy and precision of the total
161 arsenic was evaluated using a seaweed CRM and the recovery was quantitative.

162

163 Speciation analysis

164 The speciation of the hydrophilic fraction of arsenic gave the expected distribution of arsenic
165 species, with 53% of the total arsenic in the form of inorganic arsenic (62 +/- 19 mg As/kg).
166 Arsenosugars in the form of As-sugars (-glycerol, phosphate ester and sulfonate) contributed
167 32% (37 mg As/kg), while DMA was only a minor compound with less than 1 % of total As.

168

168 The arsenolipid fraction contributed also only 1.5% of total arsenic of which the majority
 169 65% was in the form of arsenosugar containing phospholipids (AsPL) (structures see Figure
 170 1). The identification and quantification was done using RP-HPLC-ICPMS/MS coupled
 171 simultaneously to ESI-MS. The assignment of the arsenic peaks was achieved by using the
 172 retention time as the first criteria, which should coexist with the corresponding protonated
 173 mass of the molecular mass (ESI-MS) as can be seen in Figure S1a and S1b (supplementary
 174 material). Further evidence for the identification were the accurate masses and MS/MS
 175 pattern as described by previously by Raab et al.^{xii}, where the arsenolipid profile of a brown
 176 seaweed *Saccharina latissima* was studied in detail.

179 **Table 1:** Total arsenic and hydrophilic arsenic species quantified; total arsenic (tAs),
 180 inorganic arsenic determined as arsenate (iAs), Sum of all arsenosugars (As-Sugar). Fractions
 181 are given as mass % of tAs. Errors are given as +/- SD for n=3.

| | tAs mg As/kg | tAs _{hydro} (hydrophilic) mg As/kg | iAs mg As/kg | DMA mg As/kg | As-Sugar (sum) mg As/kg |
|--------------------|-----------------|---|--------------------|-----------------------|-------------------------------|
| CRM CD-200* | 55 ± 1.0 | 44 ± 0.67 | 0.090 ± 0.010 | 8.6 ± 0.3 | 32 |
| <i>L. digitata</i> | 117 ± 30 | 100 ± 22 (85.5%) | 62 ± 19 (53.0%) | 0.93 ± 0.11 (0.8%) | 37 ± 3.9 (31.6%) |

*certified reference value for tAs: 55 ± 4.0 mg/kg

185 **Table 2:** Total arsenic and arsenolipids quantified; arsenic containing hydrocarbons (AsHC),
 186 arsenosugar containing phospholipids (AsPL).

| | tAs _{lipid} (lipophilic) mg As/kg | AsHC (sum) (8.2%) ^a | AsPL (sum) (65%) ^a |
|--------------------|--|--------------------------------------|-------------------------------------|
| Mass % of total As | 1.7 ± 0.22 | 0.14 | 1.1 |
| | 1.5% | 0.12% | 0.94% |

^a (% of As_{lipid})

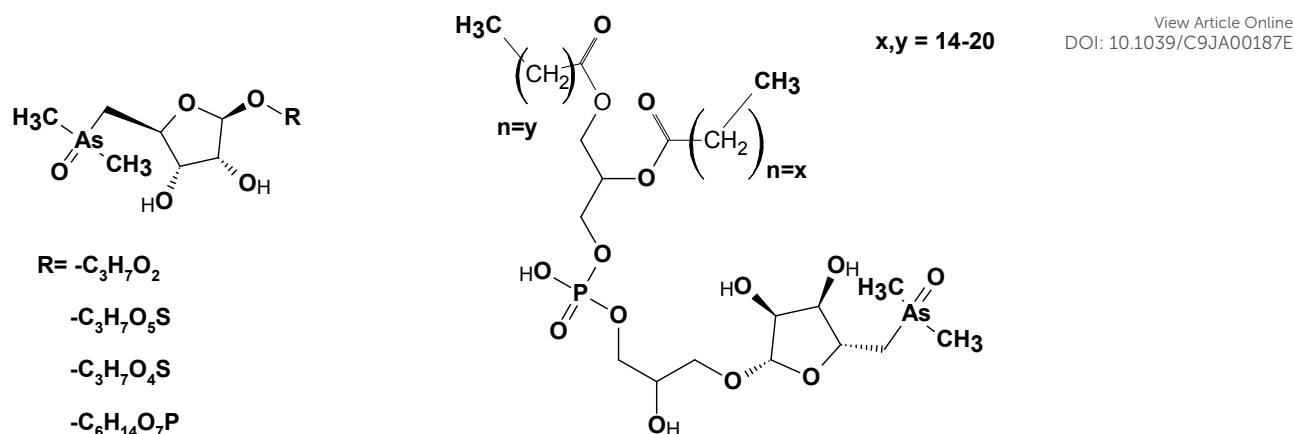


Figure 1: generic structures of major organoarsenic compounds in *L. digitata*: arsenosugar (As-sugar; left), arsenosugar containing phospholipid (AsPL; right)

Table 3: identified As-lipids and their concentration using the ICPMS signal and compound-independent quantification (n=3).

| detected arsenolipid* | detected accurate mass** | $\mu\text{g As / kg algae dry mass}$ |
|-----------------------|--|--------------------------------------|
| (AsFA422) | $\text{C}_{22}\text{H}_{36}\text{AsO}_3$ (m/z 423) | 4.2 ± 0.12 |
| (AsHC360) | $\text{C}_{19}\text{H}_{42}\text{AsO}$ (m/z 361) | 71 ± 6.7 |
| (AsHC374) | $\text{C}_{20}\text{H}_{44}\text{AsO}$ (m/z 375) | 23 ± 5.3 |
| (AsHC388 | $\text{C}_{21}\text{H}_{46}\text{AsO}$ (m/z 389) | |
| + AsHC402) | + $\text{C}_{22}\text{H}_{48}\text{AsO}$ (m/z 403) | 18 ± 2.4 |
| (AsPL930) | $\text{C}_{43}\text{H}_{84}\text{AsO}_{14}\text{P}$ (m/z 931) | 109 ± 14 |
| (AsPL944) | $\text{C}_{44}\text{H}_{86}\text{AsO}_{14}\text{P}$ (m/z 945) | 69 ± 11 |
| (AsPL958) | $\text{C}_{45}\text{H}_{88}\text{AsO}_{14}\text{P}$ (m/z 959) | 636 ± 93 |
| (AsPL972) | $\text{C}_{46}\text{H}_{90}\text{AsO}_{14}\text{P}$ (m/z 973) | 30 ± 4.4 |
| (AsPL986) | $\text{C}_{47}\text{H}_{92}\text{AsO}_{14}\text{P}$ (m/z 987) | 97 ± 13 |
| (AsPL1000) | $\text{C}_{48}\text{H}_{94}\text{AsO}_{14}\text{P}$ (m/z 1001) | 14 ± 1.7 |
| (AsPL1014) | $\text{C}_{49}\text{H}_{96}\text{AsO}_{14}\text{P}$ (m/z 1015) | 119 ± 18 |

*number in parentheses gives the non-protonated molecular mass

**For more information of the As-lipid structures see Raab et al. 2013^{vi}

TEM analysis

The cells of *L. digitata* were imaged with transmission electron microscopy (TEM) and ultra-structures such as the nucleus, Golgi apparatus, chloroplast, and vacuoles were clearly detectable (Figure 2). Most prominent, very thick cell walls were observed which are characteristic for brown algae. These cell walls are adjacent to the cell membrane and consist of an amorphous matrix of alginates and fucoidans with a fibrillary skeleton of cellulose in the inner cell wall.^{xiii,xiv} The amorphous outer cell wall can be also regarded as intercellular material.^{xv} Alginate is an unbranched anionic polysaccharide comprised of two uronic acids: mannuronic acid and guluronic acid. Fucoidans are sulphated fucose-containing

209 polysaccharides containing $-\text{SO}_3\text{H}$ groups. Cellulose accounts for only 1-8% of the algal dry
210 mass, while fucoidans and alginates represent up to 45%.^{xvi} Moreover, fucoidans play a role in
211 algal cell wall organization and could be involved in the cross linkage of alginate and cellulose.
212 Alginate gives flexibility to algae, serves as a structural support crosslinked by cationic metal
213 ions and bound to proteins, and prevents desiccation. In addition, alginate is involved in the
214 exchange of ions with seawater; it absorbs and retains polyvalent cations at concentrations
215 significantly higher than those in the surrounding water.^{xvii}



217
218 **Figure 2.** TEM image obtained from 90 nm section of resin embedded *L. digitata* cell. Image
219 is of the whole cell including, inner cell wall (cw) and amorphous outer cell wall (intercellular
220 material (In)), cell membrane, vacuoles (v), nucleus (n), nucleolus (nu), chloroplasts (ch)). Bar
221 length is 2 μm .

223 Optimization of the NanoSIMS analysis method

224 The NanoSIMS analysis method has been optimized with regard to maximal spatial/lateral
225 resolution for sub-cellular imaging and high sensitivity for detection of arsenic at trace level.
226 For high lateral resolution the Cs^+ primary ion beam was trimmed using a diaphragm (D1-4)
227 with a circled aperture of 150 μm and finally focused with the primary focusing lens (EOP) to
228 its final spot size of about 50 nm at the sample surface. This lateral resolution was confirmed
229 in our previous work by applying the knife-edge method on a standard sample^{xviii} and is in
230 agreement with the instrument specifications. In this work, the actual lateral resolution in the

231 image of the seaweed sample was determined by line scans at a sharp edge in the CN⁻ and S²⁻ images (Figures 3ib and 4iia) using the 16-84% criterion (knife-edge method). Depending on the location in the image the actual resolution was about 300 to 400 nm. Note, that in biological samples not only the NanoSIMS primary beam size, but also the structure of the sample as well as the quality of sample preparation which influences the element distribution in the sample structure contributes to the measured lateral resolution. Therefore in biological samples usually a lower resolution is measured than in standards for the knife-edge method. The selected pixel numbers (512 x 512) for a 35 µm x 35 µm image results in a theoretical pixel size of 68 nm which is slightly higher than the smallest possible probe size of 50 nm but largely sufficient in view of the measured actual lateral resolution for mapping subcellular structures in seaweed cells.

242 An advantage of the NanoSIMS is that it combines high lateral resolution with high sensitivity. 243 In order to accumulate a sufficient number of counts for the detection of trace amounts of arsenic a compromise had to be found between the dwell time of the primary beam per pixel, the number of accumulated image scans (planes), and a reasonable analysis time in which the thin sample section of 300 nm was not completely consumed. Note that NanoSIMS is a destructive technique where each scan removes sample material. Under optimized conditions a dwell time of 10 ms per pixel was chosen resulting in an image scan time of about 44 min. A long-term experiment of about 11 h 40 min showed that 16 scans were possible without complete consumption of the sample. However, already accumulation of 5 image scans enabled a sensitive arsenic detection in a reasonable analysis time of about 3 h 40 min while only a part of the sample was consumed.

253 254 *Sub-cellular elemental imaging*

255 Figures 3i-iii show high resolution imaging of a *L. digitata* cell by NanoSIMS. Both, carbon and nitrogen (via CN⁻ detection) mapping display the thick cell walls/intercellular material. The high amount of polysaccharides in these structures explains the intense carbon signal, although the cells are also embedded in a carbon containing resin matrix. The detection of nitrogen in the cell wall could indicate the presence of proteins. Nitrogen mapping showed subcellular structures, especially chloroplasts were clearly visible, probably due to higher protein concentration in the chloroplasts compared to the cytosol.

262
263 In Figure 3ii sulphur was mainly found in the thick cell walls. This intense sulphur signal can be related to the presence of fucoidans, the sulphated polysaccharides typically found in

265 seaweed cell walls of brown algae such as *L. digitata*^{xxix}. Moreover, sulphur was also detected
266 in the chloroplast which can be explained by sulphur-containing proteins involved in
267 photosynthesis, such as ferredoxin and iron-sulphur clusters.

268 The phosphorous image is an accumulation of 5 scans. P was detected in concentrated small
269 spots inside the cell which can be related to in 0.5-1 μm sized vacuoles, which can be seen as
270 electronically dense sub-cellular structures in the TEM image (Figure 2). In green algae such
271 small vacuoles are known to be acidocalcisomes containing polyphosphate and calcium and
272 are involved in osmoregulation.^{xx,xxi,xxii} Although those acidocalcisomes have never been
273 identified in brown algae, they have been found in bacteria to human cells, which make them
274 likely to occur in *L. digitata*. Moreover, phosphorus was clearly detected in the phospholipid
275 containing cell membranes adjacent to the cell walls.

277 In Figure 3iii arsenic was found in a pattern consistent with the cell wall/intercellular material.
278 The image is an accumulation of 5 scans. Figure 3iii (b and c) are a colour merge images of the
279 relative distribution of arsenic (white) and nitrogen (red) or phosphorus (blue). It further
280 demonstrates that the arsenic is mainly present in the cell wall with phosphorus outlining the
281 cell membranes and subcellular structures.

283 Knowing the arsenic speciation in *L. digitata*, it is not expected that all arsenic would be in the
284 cell membrane, since only a small proportion of arsenic is lipophilic (1.5%). Almost all arsenic
285 is in the form of either inorganic arsenic or in the form of hydrophilic arsenosugars (together
286 approx. 82%). No arsenic was detected inside the cells by NanoSIMS in either the cytosol, the
287 vacuoles or acidocalcisomes (their location was indicated by the phosphorus map). Hence, the
288 localisation of arsenic in *L. digitata* is significantly different to the accumulation of arsenic in
289 rice root cells.^{xxiii} Inorganic arsenic in rice roots is bound mainly to phytochelatins while DMA
290 seemed unbound.^{xxiv} In contrast brown seaweed with a large proportion of inorganic arsenic
291 (*Hijiki* spp.) showed no significant amounts of arsenic phytochelatin complexes.^{xxv} Hence, the
292 lack of arsenic in the cytosol and in particular in the vacuoles of *L. digitata* is not surprising.

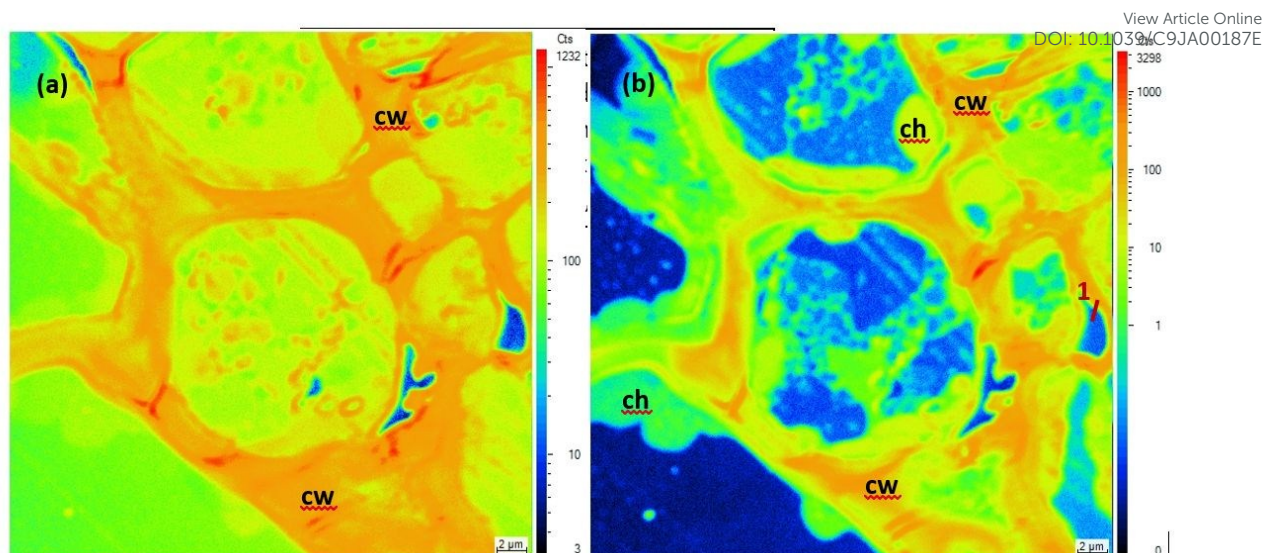
294 It seems that most arsenic is located in the cell walls containing polysaccharides such as
295 alginate, fucoidan and cellulose. Those alginates are also known to accumulate mono and
296 divalent cations such as Na^+ , K^+ , Ca^{2+} , but also Zn^{2+} and Cu^{2+} .^{xiv} Arsenic however in its
297 inorganic forms is either neutral ($\text{As}(\text{OH})_3$) or anionic (HAsO_4^{2-}) and will not bind to the
298 alginates in the same way. So far it is not known if arsenate or arsenite bind to either alginates

299 or fucoidans, which are abundant in the cell walls in brown seaweed. The fucoidans however
300 bind sulphate as sulfuric acid ester. If arsenic binds as arsenate to the carbohydrate in a similar
301 way is unclear. The resulting arsenic acid esters would be very unstable and will quickly
302 hydrolyse and form again inorganic arsenic.^{xxvi} It has been noted that not only AsHC and AsPL
303 can be extracted, some unstable arsenic species have also been extracted with DCM/MeOH. A
304 significant part of the extract eluted however in the void of a reverse phase HPLC method. This
305 was likely to be attributed to unstable non-polar arsenolipids as shown before.^{xxvii} Arsenic acid
306 esters would quickly hydrolyse to inorganic arsenic during the sample preparation step.

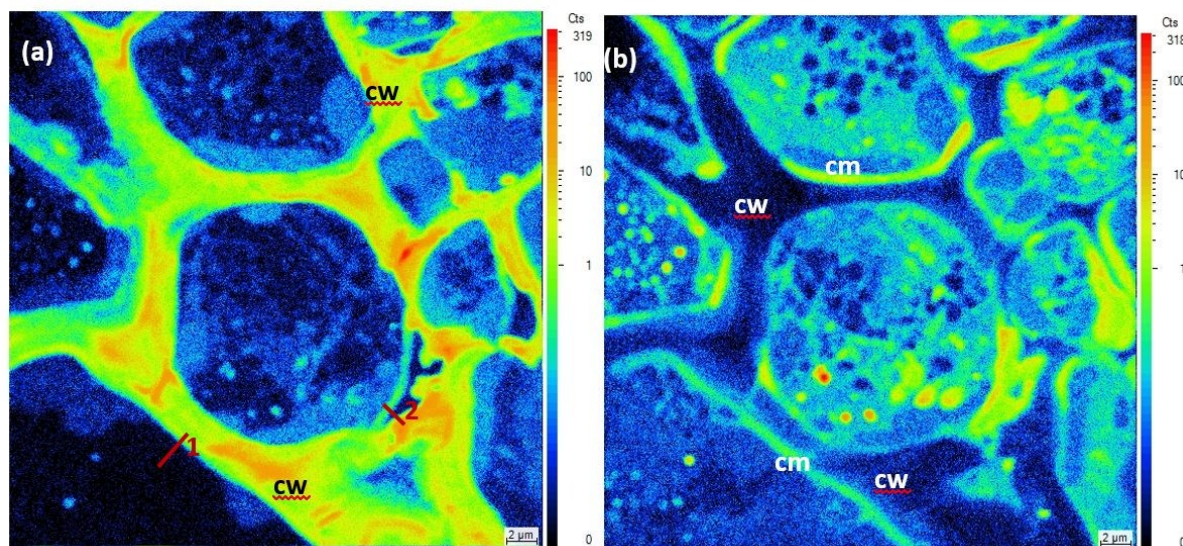
307
308 Although the binding of arsenite or arsenate to the constituents of the cell wall and membrane
309 is unclear, the accumulation of arsenate into the cell wall is however mechanistically
310 conceivable. The arsenic accumulation into brown seaweed depends on the salinity and hence
311 also on the arsenic concentration in the seawater.^{xxviii} Arsenate might directly accumulate from
312 seawater or indirectly when it is taken up through phosphate transporters and then excreted as
313 arsenite. Efflux of arsenite is well known, while the efflux of arsenate has only recently been
314 suggested to occur as well.^{xxix}

315
316 The accumulation of arsenosugars in the cell wall is however more difficult to understand.
317 Since no arsenosugars have been found in seawater so far, the accumulation of these arsenic
318 species need to come from biotransformation reactions either directly within the macroalgae or
319 from bacteria on the surface of the seaweeds.^{xxx} If the arsenosugars are transported through the
320 cell membrane into the cell wall, then certain transporters which excrete those compounds need
321 to exist. Otherwise, the arsenosugars could be linked to the alginates which are produced in the
322 Golgi apparatus and then directly incorporated into the carbohydrate structure. They might bind
323 directly to the carbohydrates via the alcohol groups or the sulfonate (major arsenosugar in *L.*
324 *digitata* is the AsSugar-SO₃). These compounds again would be rather unstable in water and
325 hydrolyse quickly. The fact that no hotspot inside the cell which could be assigned to the Golgi
326 apparatus has been found, indicates that the arsenic transformation inside the cell needs to be
327 fast. Alginate generation is taking place within 20 minutes. This would explain that the cytosol
328 and the sub-cellular structures inside the cell are virtually arsenic free.

329
330

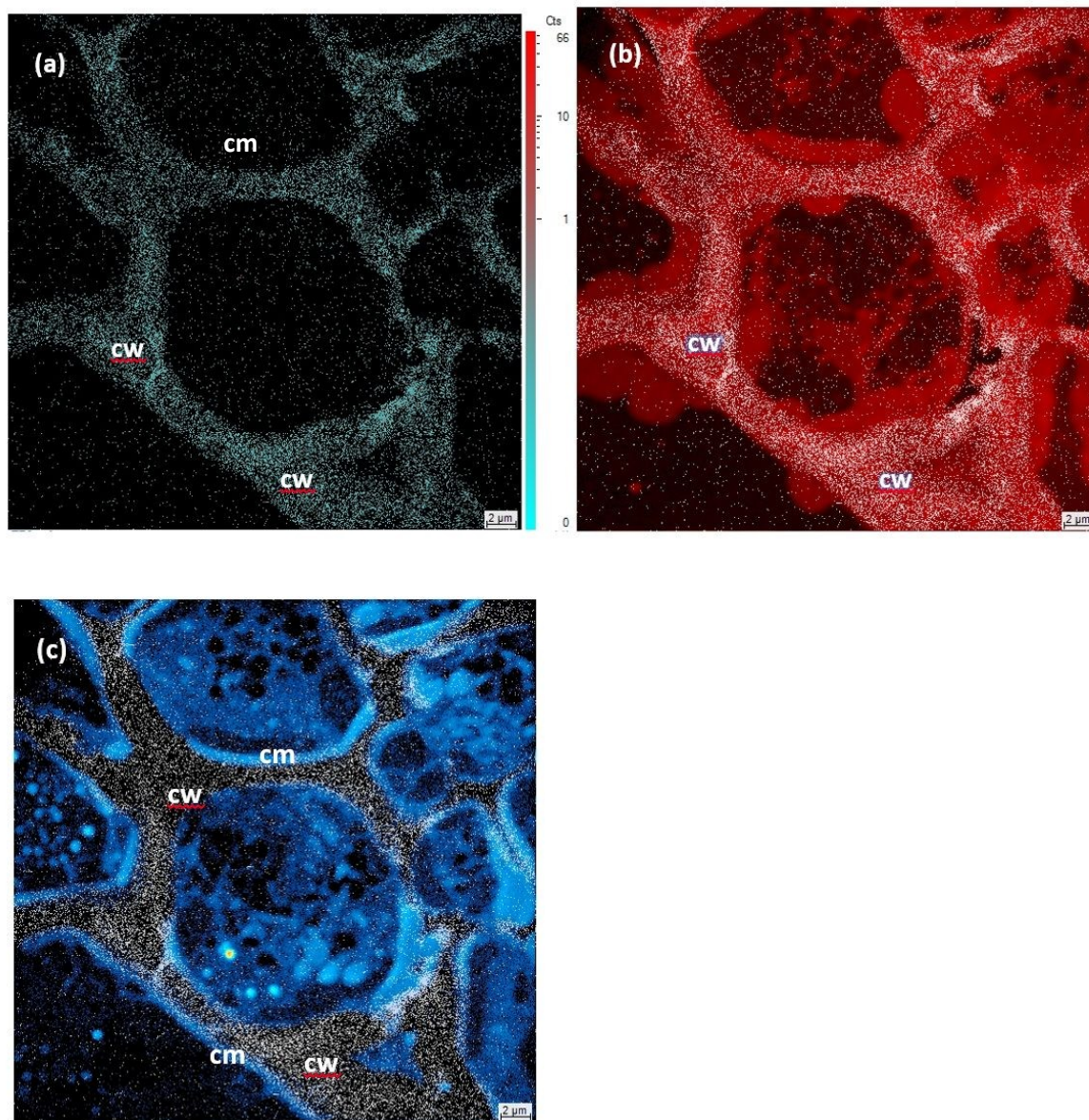


331
 332 **Figure 3i.** High resolution imaging of carbon (via C_2^-) (a) and nitrogen (via CN^-) (b) in *L.*
 333 *digitata* cells by NanoSIMS obtained from a 300 nm resin section. Both images display the
 334 thick cell walls (cw). N mapping (b) shows subcellular structures, e.g. chloroplasts (ch), line
 335 scan 1 (red line) resulted in a measured lateral resolution of 305 nm. NanoSIMS images were
 336 obtained with an Cs^+ plasma primary ion source for detection of negative secondary ions: 35 x
 337 35 μm^2 field of view images; 512 x 512 pixel; dwell time 10 ms/pixel; total image acquisition
 338 time approx. 44 min.



339
 340 **Figure 3ii.** High resolution imaging of S (a) and P (b) in *L. digitata* cells by NanoSIMS
 341 obtained from a 300 nm resin section. S is mainly concentrated in the thick cell
 342 walls/intercellular material (cw). P is more concentrated in spots inside the cells as well as in
 343 the cell membrane (cm) adjacent to the cell wall. Line scans 1 and 2 (red lines) resulted in
 344 measured lateral resolutions of 433 nm and 295 nm, respectively. NanoSIMS images were

345 obtained with an Cs⁺ plasma primary ion source for detection of negative secondary ions: 35 x
 346 35 μm² field of view images; 512 x 512 pixel; dwell time 10 ms/pixel; total image acquisition
 347 time approx. 44 min.



348

349

350 **Figure 3iii.** High resolution accumulated imaging of As (a) in *L. digitata* cells and two colour
 351 merge images that shows the relative distribution of As (white) and N (red) localisation (b) as
 352 well as As (white) and P (blue) localisation (c) by NanoSIMS obtained from a 300 nm resin
 353 section. As was mainly found in the cell wall/intercellular material (cw) and to a much lesser
 354 extend in the cell membrane (cm). NanoSIMS images were obtained with an Cs⁺ plasma
 355 primary ion source for detection of negative secondary ions: 35 x 35 μm² field of view images;
 356 512 x 512 pixel; dwell time 10 ms/pixel; total image acquisition time approx. 44 min.

357

1
2
3 358 It has been speculated that arsenosugars are intermediates in the formation of arsenolipids such
4 as AsPL.ⁱⁱ But when arsenosugars accumulate in large quantities in the cell wall, then the
5 biosynthesis to AsPL needs to take place there as well, which is unlikely. Hence, the
6
7 360
8
9 361 localisation of arsenic in the cell wall rather than in the cell membrane indicates that the
10 seaweed can handle certain concentrations of arsenic and has means of excluding the arsenic
11
12 362 from the cytosol and other sub-cellular structures within the cell. The biotransformation and
13
14 363 kinetics of arsenic in *L. digitata* are not clear, but the seaweed is able to biotransform quickly
15
16 364 the taken up arsenic and transport it outside the cell. This could be an effective detoxification
17
18 365 strategy, or the evidence of the utilization of the accumulated arsenic for a purpose, since the
19
20 366 cell wall with the gel-like alginates and sulphated fucoidans act often as the first barrier to toxic
21
22 367 or unwanted chemicals. More fundamental studies are necessary to elucidate the biochemical
23
24 368 role of arsenic in seaweed.
25
26 369

27
28 370
29
30 371 In summary the complimentary use of high spatial resolution imaging of elements at a sub-
31
32 372 cellular level in combination of speciation analysis can shed new lights on the role of arsenic
33
34 373 in seaweeds. Is the arsenic in the form of inorganic arsenic essential for the algae as suggested
35
36 374 elsewhere^{xxxi} or is the efflux of arsenic in these molecular forms into the intercellular space or
37
38 375 the cell wall a successful detoxification strategy? These questions can only be asked if in
39
40 376 addition to arsenic speciation also its distribution within a cell and sub-cellular structures is
41
42 377 known this however would need a high resolution imaging technique which is capable at the
43
44 378 same time to provide speciation information. μ -XANES would have the analytical attributes
45
46 379 but its resolution is currently not sufficient to identify subcellular structures.
47
48 380

49 381

50 382

51 383 **References**

- 52
53
54
55
56
57
58
59
60
- ⁱ H.R. Hansen, A. Raab and J. Feldmann, *J. Anal. At. Spectrom.* 2003, **18**, 474-479.
ⁱⁱ X.M. Xue, J. Ye, G. Raber, B.P. Rosen, K. Francesconi, C. Xiong, Z. Zhu, C. Rensing, and Y.G. Zhu, *Environ. Sci. Technol.* 2019, **53**, 634-641.
ⁱⁱⁱ W. Maher and E. Butler, *Appl. Organomet. Chem.*, 1988, **2**, 191-214.
^{iv} J. Feldmann and E.M. Krupp, *Anal. Bioanal. Chem.*, 2011, **399**, 1735-1741.
^v S. Garcia-Salgado, G. Raber, R. Raml, C. Magnes and K.A. Francesconi, *Environ. Chem.*, 2012, **9**, 63-66.

- vi A. Raab, C. Newcombe, D. Pitton, R. Ebel, and J. Feldmann, *Anal. Chem.* 2013, **85**, 2817-2824.
- vii K. Hanaoka, K. Yosida, M. Tamano, T. Kuroiwa, T. Kaise and S. Maeda, *Appl. Organomet. Chem.*, 2001, **15**, 561-565.
- viii J.M. Ronan, D.B. Stengel, A. Raab, J. Feldmann, L. O’Hea, E. Bralatei and E. McGovern. *Chemosphere* 2017, **186**, 17-23.
- ix E. Bralatei, K. Nekrosuite, J. Ronan, A. Raab, E. McGovern, E.M. Krupp and J. Feldmann, *Microchim. Acta* 2017, **184**, 1701-1709.
- x A.H. Petursdottir, N. Friedrich, S. Musil, A. Raab, H. Gunnlaugsdottir, E.M. Krupp and J. Feldmann, *Anal. Met.* 2014, **6**, 5392-5396.
- xi K.O. Amayo, K.O, A.H. Petursdottir, C. Newcombe, H. Gunnlaugsdottir, A. Raab, E. Krupp, and J. Feldmann, *Anal. Chem.* 2011, **83**, 3589-3595.
- xii A. Raab, C. Newcombe, D. Pitton, R. Ebel and J. Feldmann, *Anal. Chem.* 2013, **85**, 2817-2824.
- xiii S. Schiewer and B. Volesky, Biosorption by marine algae. In: Valdes JJ, editor. Remediation. Dordrecht, The Netherlands: Kluwer Academic Publishers; 2000.p. 139–69.
- xiv T. A. Davis et al., A review of the biochemistry of heavy metal biosorption by brown algae. *Water Res.* 2003, **37**, 4311–4330.
- xv W. Mackie and R.D. Preston. Cell wall and intercellular region polysaccharides. In: W.D.P. Stewart, editor. Algal physiology and biochemistry. Oxford, UK: Blackwell Scientific Publications; 1974. p. 58–64.
- xvi K. L. Moore, M. Schroder, Z. Wu, B. G. H. Martin, C. R. Hawes, S. P. McGrath, M. J. Hawkesford, J. Feng Ma, F.-J. Zhao, and C. R. M. Grovenor, *Plant Physiol.*, 2011, **156**, 913–924.
- xvii H. Jiang, C. N. Goulbourne, A. Tatar, K. Turlo, D. Wu, A. P. Beigneux, C. R. M. Grovenor, L. G. Fong, and S. G. Young, *J. Lipid Res.*, 2014, **55**, 2156–2166.
- xviii Malherbe, J., Penen, F., Isaure, M.-P., Frank, J., Hause, G., Dobritzsch, D., Gontier, E., Horreard, F., Hillion, F., Schaumloeffel, D., *Anal. Chem.* 2016, **88**, 7130–7136
- xix A. Synytsya, J. Čopíková, W.J. Kim, Y.I. Park. (2015) Cell Wall Polysaccharides of Marine Algae. In: Kim SK. (eds) Springer Handbook of Marine Biotechnology. Springer Handbooks. Springer, Berlin, Heidelberg.
- xx N. Lander, C. Cordeiro, G. Huang and R. Docamo, *Biochem. Sco. Trans.* 2016, **44**, 1-6.
- xxi F. Penen, M.P. Isaure, D. Dobritzsch, I. Bertalan, H. Castillo, O. Proux, E. Gontier, P. Le

Coustumer and D. Schaumlöffel, *Metallomics* 2017, **9**, 910-923.

xxii F.A. Ruiz, N. Marchesini, M. Seufferheld, Govindjee and R. Docampo, *J. Biol. Chem.*, 2001, **276**, 49196-46203.

xxiii K.L. Moore, M. Schroder, E. Lombi, F.J. Zhao, S.P. McGrath, M.J. Hawkesford, P.R. Shewry and C.R.M. Grovenor, *New Phytol.* 2010, **185**, 434-445.

xxiv B.L. Batista, M. Nigar, A. Mestrot, B.A. Rocha, F. Barbosa Jr, A.H. Price, A. Raab and J. Feldmann, *J. Exp. Bot.*, 2014, **65**, 1467-1479.

xxv B.A. Wood, A.A. Meharg, S. Miyashita, T. Kaise, A. Raab and J. Feldmann, *Environ. Chem.* 2011, **8**, 30-43.

xxvi F.H. Westheiner, *Science* (1987) **235**, 1173-1178.

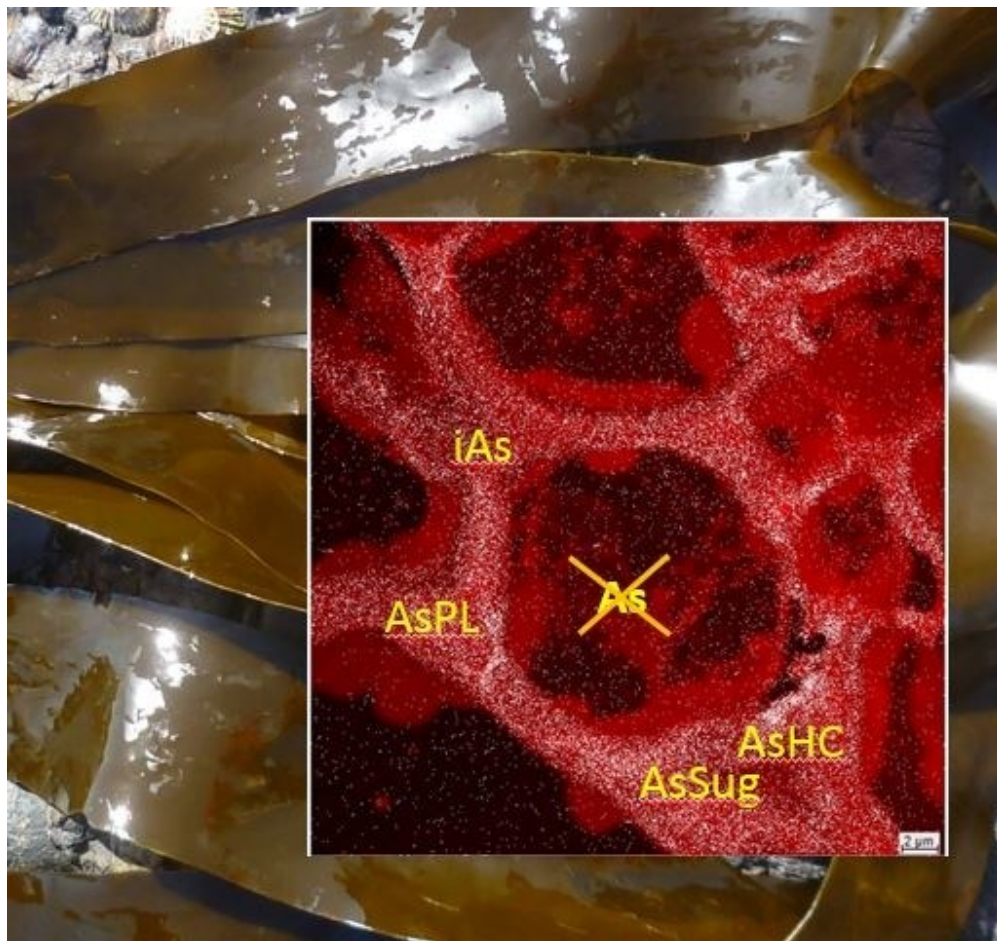
xxvii A.H. Petursdottir, J.R. de Jesus, H. Gunnlaugsdottir and J. Feldmann, *J. Anal. At. Spectrom.*, 2018, **33**, 102-110.

xxviii E. Ownsworth, D. Selby, C.J. Ottley, E. Unsworth, A. Raab, J. Feldmann, A.D. Sproson, J. Kuroda, C. Faidutti and P. Bucker, *Sci. Tot. Environ.*, 2019, 685, 259-272.

xxix L.D. Garinski, B.P. Rosen and J. Chen, *Environ. Intern.*, 2019, **126**, 585-597.

xxx A.H. Petursdottir, J. Bladgen, K. Gunnarsson, A. Raab, D.B. Stengel, J. Feldmann, H. Gunnlaugsdottir, *Anal. Bioanal. Chem.*, 2019, **411**, 4973-4985.

xxxi A.H. Petursdottir, K. Fletcher, H. Gunnlaugsdottir, E. Krupp, F. Kuepper, J. Feldmann, *Environ. Chem.*, 2015, **13**, 21-33.



108x101mm (120 x 120 DPI)

1
2
3
4
5
6
7
8
9
10
11
12
13
14
15
16
17
18
19
20
21
22
23
24
25
26
27
28
29
30
31
32
33
34
35
36
37
38
39
40
41
42
43
44
45
46
47
48
49
50
51
52
53
54
55
56
57
58
59
60